J Nanostruct 15(3): 1230-1244, Summer 2025

RESEARCH PAPER

Synthesis, Characterization, and Comparative Study of Novel Ternary PANI/rGO-Cr_2O_3, PANI/rGO-NiO, PANI/NiO-Cr_2O_3 Nanocompsites for Dielectric and Thermal Application

Amir F. Dawood AL-Niaimi, Kawther Taha Muhammed *

Department of Chemistry, College of Science, University of Diyala, Diyala, Iraq

ARTICLE INFO

Article History:
Received 19 March 2025
Accepted 26 June 2025
Published 01 July 2025

Keywords:
Electrical conductivity
PANI/NiO-Cr_2O_3
PANI/rGO-Cr_2O_3
PANI/rGO-NiO
Thermal application

ABSTRACT

This study involved the preparation of novel ternary PANI/rGO-Cr_2O_3, PANI/rGO-NiO, PANI/NiO-Cr_2O_3 nanocompsites using in-situ polymerization method. The resulting nanocomposites were identified using FT-IR, XRD, and FESEM measurements. The electrical properties of single PVA polymer films and PVA hybrids were studied by LCR techniques at frequency range of 1kHz -5kHz and a temperature of 25 °C. The measurements of electrical conductivity exhibited an augmentation in the magnitudes of the dielectric constant (ε') and the dielectric loss factor (ε''). The value decreases as the frequency increases. The thermal measurements showed that the thermal conductivity coefficient decreases with increasing the frequencies.

How to cite this article
AL-Niaimi A., Muhammed K. Synthesis, Characterization, and Comparative Study of Novel Ternary PANI/rGO-Cr_2O_3, PANI/rGO-NiO, PANI/NiO-Cr_2O_3 Nanocompsites for Dielectric and Thermal Application J Nanostruct, 2025; 15(3):1230-1244. DOI: 10.22052/JNS.2025.03.040

INTRODUCTION

Advancements in materials science have greatly influenced the electrical and industrial properties of materials used in energy storage [1]. Due to superior electrochemical properties, low cost, environmentally friendly nature, high stability and simplicity of synthesis, polyaniline and its derivatives are crucial materials developed for energy storage applications [2, 3]. Nevertheless, this particular polymer exhibits subpar mechanical qualities and limited process ability [1, 4]. However, it is possible to overcome these limitations and enhance the electrical, mechanical, and thermal properties of conductive polymers by employing carbon nanostructures like graphene, graphene oxide (GO), carbon nanotubes, and metal oxides [5-8]. Recently, graphene has attracted a lot of attention because of its extraordinary mechanical, thermal, and electrical capabilities, which allow it to significantly improve the properties of polymer-based nanocomposites. The attributes stem from its honeycomb-like configuration, which enhances its distinctive properties. The properties arise from its honeycomb-like structure, characterized by the thickness of a single carbon atom and a high density of structural components [9, 10]. Graphene oxide is a complex hydrocarbon network with a multicyclic layer that is partially aromatic. Furthermore, it lies in the production of nano-electronic devices and sensors. Metal oxides

* *Corresponding Author Email: scichemms232412@uodiyala.edu.iq*

nanoparticles demonstrate characteristics of semiconductors. The NiO, and Cr_2O_3 nanoparticle are solid powders that are insoluble in water (H_2O) but can slowly dissolve in NH_4Cl, dilute acid, and ammonia solution [11]. The current investigation involved the preparation of a ternary polymeric nanocomposite consisting of PANI/rGO-Cr_2O_3, PANI/rGO-NiO, and PANI/NiO-Cr_2O_3. The products were characterized using techniques such as FTIR, XRD, FESEM. Finally, the electrical characteristics and thermal conductivity of these materials were examined.

MATERIALS AND METHODS

Synthesis of graphene oxide

GO was produced by the modified Hummer technique. The graphite (Alpha, 95%) was mixed with concentrated H_2SO_4 (MERCK, 95%) and $KMnO_4$ (Alpha, 95.5%) in a beaker. The mixture was stirred continuously for 20 min, and then heated to 98 °C. Non-ionic water was added, followed by H_2O_2 (HIMEDIA, 30%). The mixture turned yellow, washed with HCl (THOMAS BAKER, 35%) and non-ionic water, and dried at 70 °C for 4 h [12, 13].

Synthesis of reduced graphene oxide (rGO)

rGO was prepared by chemical reduction of an aqueous solution of GO in 250mL of deionized water using an ultrasonic device for 30 min. After that, 5mL of hydrazine hydrate was added to the flask and left for the sublimation process reverse reflux for 24 h at 90 °C. The mixture was filtered and the precipitate was washed with deionized water several times. Finally, it was dried for 24 h at 90 °C [13, 14].

Synthesis of PANI

1.5 mL of purified aniline (LOBALA Chemie/India, 99%) was placed in a beaker with a capacity of 50 mL. The beaker was then placed in an ice bath at a temperature of 0°C for a duration of 10 min. Next, 20 mL of HCl 1 M was slowly added into above solution while continuously stirring for 20 min. This was followed by the addition of ammonium persulphate APS (MERCK, 99.5%) at 0°C. The solution was thereafter agitated for duration of 2 h in an ice bath, and subsequently stored overnight in the refrigerator. The precipitate underwent filtration and was thereafter washed 4 times with distilled water and ammonium hydroxide NH_4OH (LOBALA Chemie/India, 25%). This was followed by further washing with distilled water until the pH reached neutrality. Ultimately, the solid residue was subjected to a drying process at a temperature of 80°C for a duration of 2 h [15-17].

Synthesis of extract

1 g of both extracts (ground ginger and ground cumin) were taken and each of them was placed in 50 mL of water on the thermal heater while continuously stirring for 15 min. Then, the temperature was raised for 1 h. The sediment was then separated from the solution.

Synthesis of NiO and Cr_2O_3

1 g of aqueous nickel nitrate and chromium (III) nitrate were separately dissolved in 25 mL of water. Then, 10 mL of extracts were added in a burette, followed by the addition of NH_4OH until PH reached 10 for NiO and PH reached 8 for Cr_2O_3. Then the precipitate was washed 4 times, dried and then placed in an oven at 500°C for 3 h.

Synthesis of rGO-NiO, rGO-Cr_2O_3, Cr_2O_3-NiO

The rGO-NiO was synthesized by dispersing 1 g of rGO in 200 mL of water using an ultrasonic water bath at 25°C for 1 h, resulting in a solution of rGO. Subsequently, 0.7g of NiO was added into the rGO solution and stirred for 1 h at 25°C. The precipitate was separated using centrifugation. Finally, the precipitate was dried at 90°C for 4 h [18]. The similar conditions were employed for fabrication of rGO-Cr_2O_3 and Cr_2O_3-NiO.

Synthesis of PANI/rGO-Cr_2O_3, PANI/rGO-NiO, and PANI/NiO-Cr_2O_3

The ternary nanocomposite was synthesized by dispersing 0.5 g of the binary composite rGO-NiO, rGO-Cr_2O_3 and Cr_2O_3-NiO in 50 mL of non-ionic water using an ultrasonic bath at a temperature of 25°C for 1 h. Subsequently, the resulting mixture was combined with 1 g of PANI dissolved in 100 mL of 0.1M HCL. Then, a solution of an oxidizing agent by dissolving 6 g of APS in 100 mL of 0.1M HCI was fabricated. This solution was introduced into the main mixture while vigorously stirring for 12 h at 25°C. Next, the sediment was washed and then dried in the oven at 80°C for 4 h.

Synthesis of PANI/rGO-Cr_2O_3, PANI/rGO-NiO, and PANI/NiO-Cr_2O_3 nanocomposite membranes

The nanocomposite membranes were fabricated by incorporating diverse weight percentages of the PANI/rGO-Cr_2O_3, PANI/rGO-NiO,

and PANI/NiO-Cr_2O_3 nanocomposite. A solution containing a specified amount of PVA in 20 mL of distilled water was combined with (2-10%) of ternary nanocomposite in 3 mL of distilled water. The combination was agitated at a temperature of 60 °C until a noticeable alteration occurred in the mixture. The sample was subjected to sonication (405 Power China) for 15 min at a temperature of 25 °C, followed by the process of casting onto a glass mold.

Dielectric constant measurement

In order to determine the dielectric properties of the produced films, a circular piece with a diameter of 3 cm was cut from the film. This was done to match the diameter of the electrodes in the LCR meter (Impedance Analyze Agilent 50Hz-5mHz). Dielectric investigations were conducted at several frequencies ranging from 1 to 5 KHz at a temperature of 25 °C. the dielectric constant (ε′), dielectric loss factor (ε′′) were calculated according the Eq. 1 [13, 19]:

$$\varepsilon' = \frac{Cd}{\varepsilon_0 A} \quad (1)$$

Where, ε_0 is permittivity of the vacuum (F/m), which is equal to 8.85 x 10^{-12}. d (m) denotes the distance between the two conducting plates. A (m^2) is conductive plate's surface area. C **(**F) denotes the capacity in the presence of a vacuum (Eq. 2).

$$\tan\delta = \frac{\varepsilon''}{\varepsilon'} \quad (2)$$

Where tan δ is dissipation factor. The K value can be computed using the Eq. 3

$$K\left\{\frac{T_B - T_A}{d_S}\right\} = e\left\{T_A + \frac{r}{2}\left(d_A + \frac{d_S}{4}\right)T_A + d_S\frac{T_B}{2r}\right\}$$

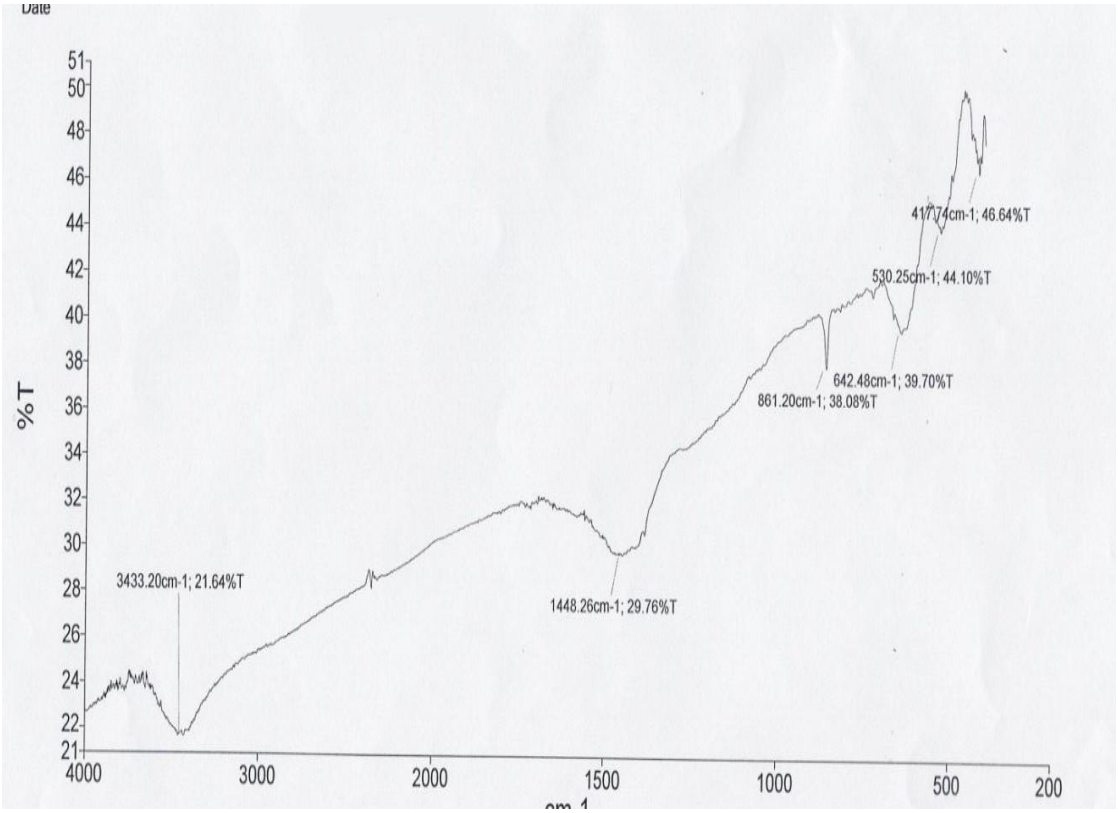

Fig. 1. FTIR spectrum of rGO.

Where, T_A, T_B, T_C indicates the temperature of disk A, B, and C, correspondingly. d (m) is disc's thickness. r (m) is disk's radius. I (A) show the current passed via heating coils. V (v) is the heating coil's potential difference on both ends.

RESULTS AND DISCUSSION

FTIR analysis

Fig. 1 presents the FTIR spectrum of rGO. The distinct bands observed at 3433.95, 1641.1, and 1115.19 cm^{-1} are associated with vibrational frequencies of the O–H, C=C, and C–O groups in the carbon-hydroxyl groups [20].

Fig. 2 shows the FTIR spectrum of PANI. The peak at 3434.13cm^{-1} is attributed to N-H stretching vibrations. The peaks at 1558.40cm^{-1} and 1475.47cm^{-1} are attributed to the stretching vibrations of quinoid and benzenoid ring of PANI, respectively. Moreover, the characteristic of N=Q=N and the stretching vibration of C=C were appeared at 1104.55cm^{-1} and 1293.88cm^{-1}. Band at 797.17 cm^{-1} is attributed to C-H aromatic ring [21].

To understand the dominant functional group present in the catalyst, FTIR spectrum was recorded at room temperature. The FTIR spectrum of NiO is shown in Fig. 3. Peak around the 418.80 cm^{-1} is because of the Ni-O bond stretching vibrations. The absorption band at 1637.87 cm^{-1} is due to the symmetric and the asymmetric stretching mode of vibrations of the CO_2 molecule absorbed from the air [22]. Also, the broad peak at 3437.01 cm^{-1} may be because of stretching and bending vibrations of –OH group absorbed on catalyst surface from the atmosphere when FTIR analysis was carried out [23].

FTIR spectrum of rGO-NiO nanocomposite is shown in Fig. 4. The main peaks detected at 3434.25, 1629.04, 1125.26, 423.02, and 630.89 cm^{-1} are recognized to the O–H, C –C, C–OH, C–C, and C–O, respectively. Because of the partially reduction of oxygenated functional

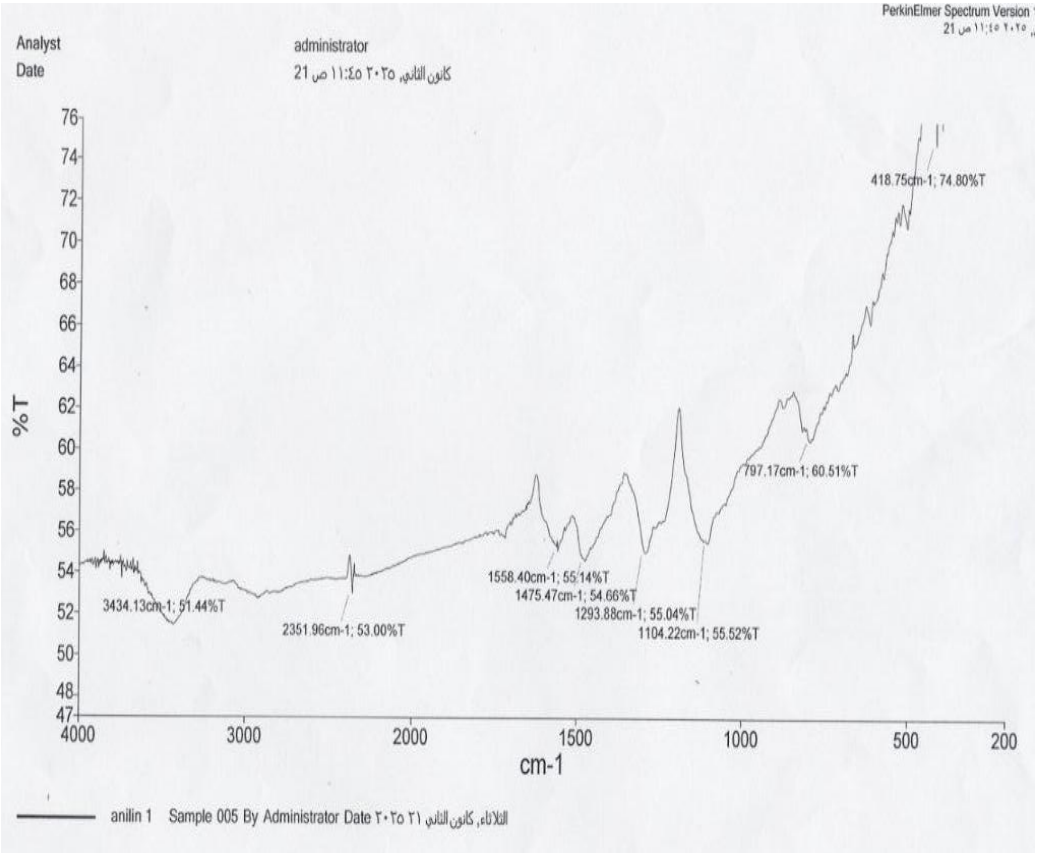

Fig. 2. FTIR spectrum of PANI.

groups during the reaction, the intensities of these peaks reduced dramatically following the formation of NiO nanoparticles on rGO sheets. Indeed, after reducing GO with NH_4OH, the peaks caused by O–H, C–O, and C–O stretching reduced considerably.

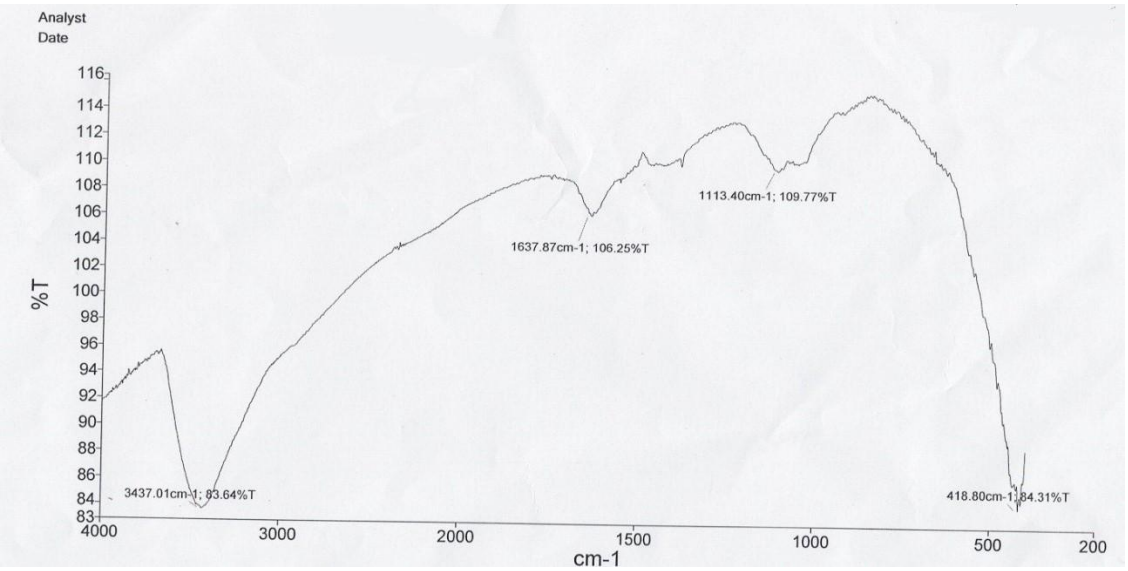

Fig. 3. FTIR spectrum of NiO.

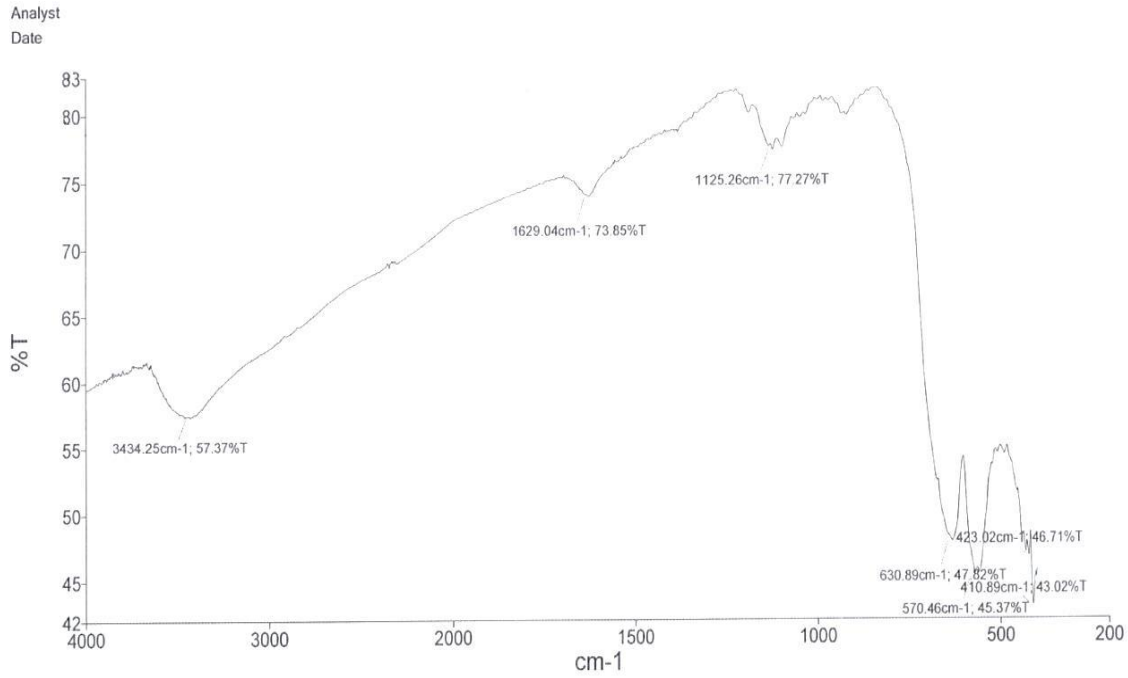

Fig. 4. FTIR spectrum of rGO-NiO nanocomposite.

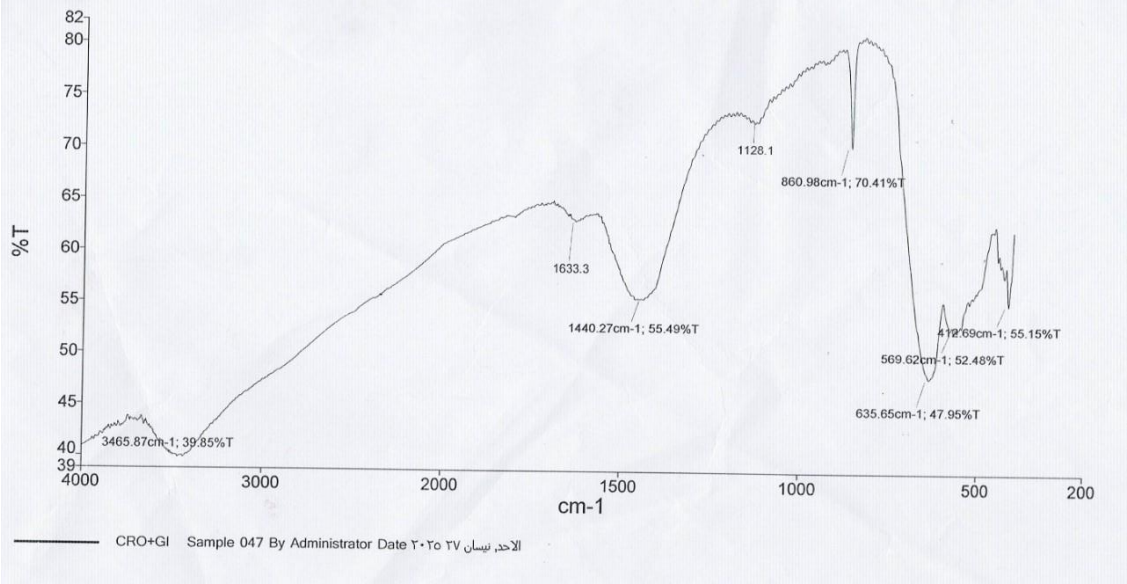

Fig. 5. FTIR spectrum of rGO-Cr_2O_3 nanocomposite.

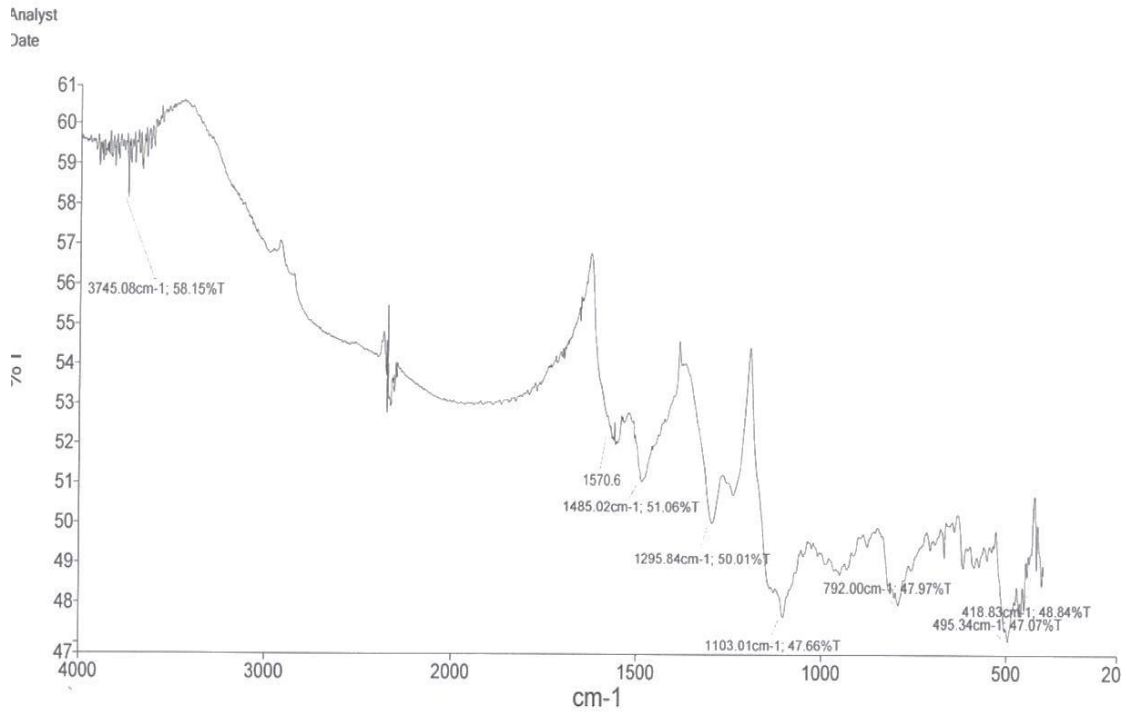

Fig. 6. FTIR spectrum of NiO-Cr_2O_3 nanocomposite.

Fig. 5 illustrates the existence of numerous distinct bands for the hybrid composite, with absorption bands in the range of 3364.25cm^{-1} attributed to the NH_2 group, and prominent bands in the range of 1508.15-1582.05cm^{-1} corresponding to the C=C group, associated with the extension of cyclic compounds and selective vibrations. The absorption band at 1218.89cm^{-1} corresponds to the C-N in the quinoid and benzoid groups, while the band at 1046.57cm^{-1} is associated with the alkoxy and epoxy groups. Furthermore, the band located at 422.12cm^{-1} corresponds to the Cr-O group.

The FTIR spectrum of NiO-Cr_2O_3 nanocomposites is shown in Fig. 6. A broad band at 3420 cm^{-1} corresponds to the stretching modes of surface

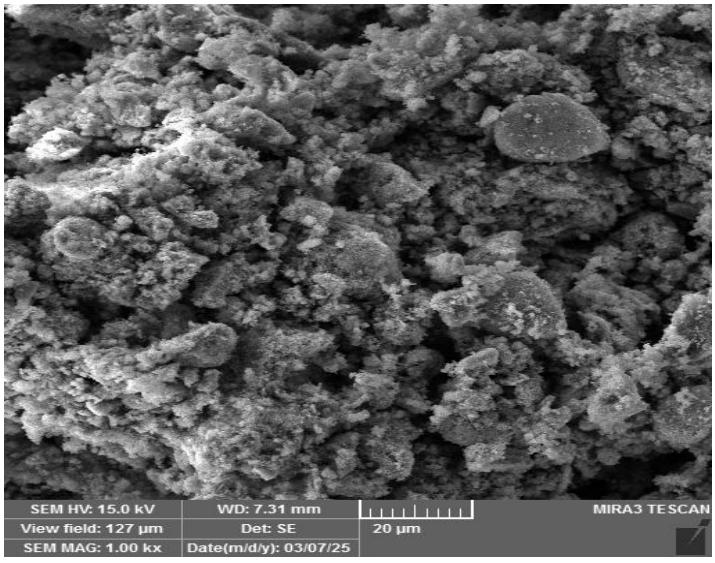

Fig. 7. FESEM image of rGO.

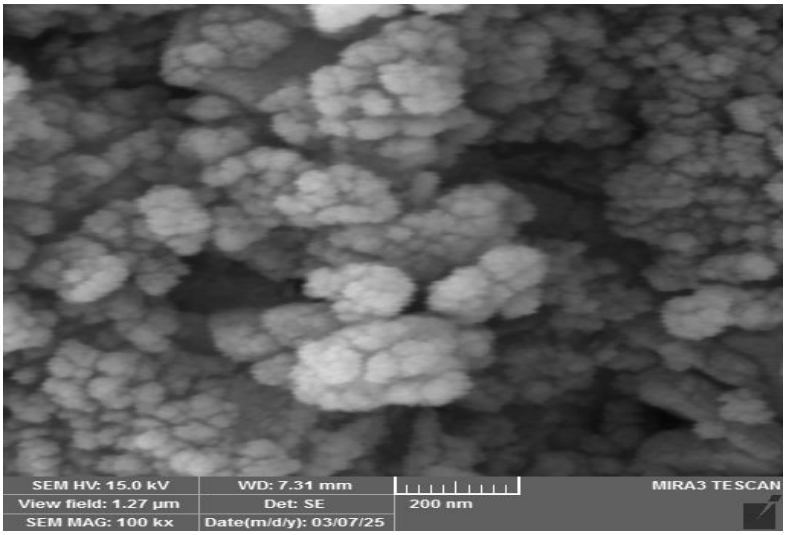

Fig.8. FESEM image of Cr_2O_3.

OH groups. Metal oxide generally reveals absorption bands below 1000 cm^{-1} due to inter-atomic vibrations. Two sharp peaks displayed at 652 and 562 cm^{-1} attributed to Cr-O stretching modes, which are clear evidence for the presence of the crystalline Cr_2O_3 [24]. Interestingly, it was

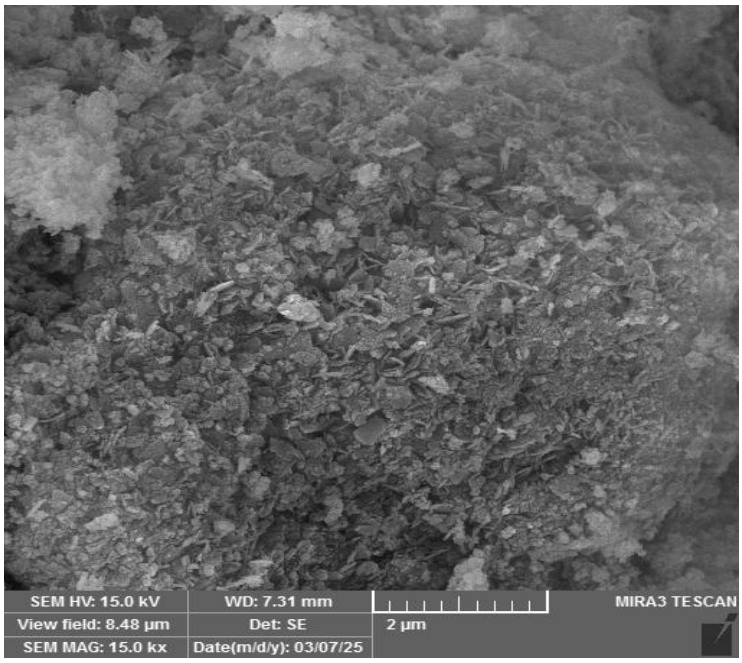

Fig. 9. FESEM image of PANI.

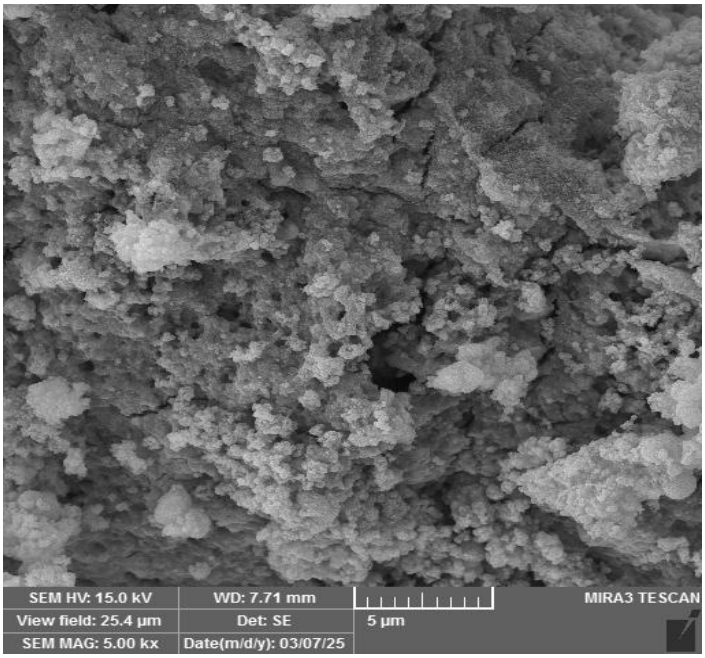

Fig. 10. FESEM image of rGO-NiO.

observed that intensity of the higher frequency decrease with enhancement in NiO concentration.

FESEM analysis

The FESEM image of rGO in Fig. 7 displayed some distortions on the layer's surface. This is due to the reduction by hydrazine hydrate.

SEM micrograph of Cr_2O_3 is shown in Fig. 8. It can be seen that the sample is spherical and particles are agglomerated at the surface.

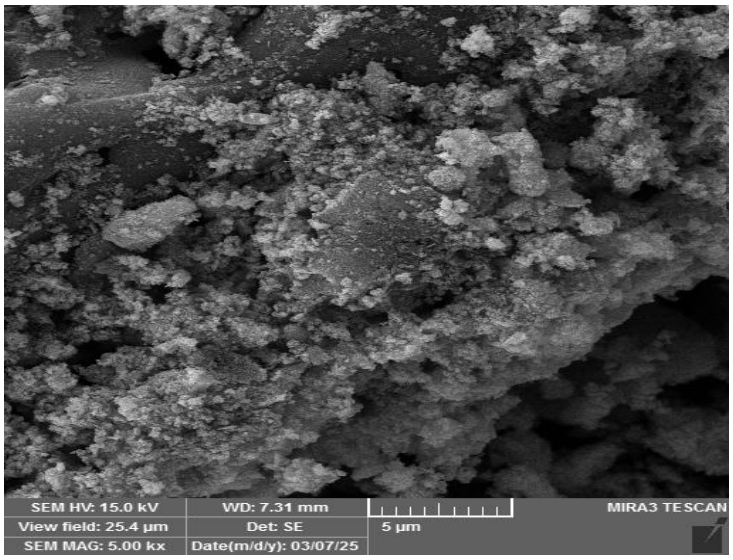

Fig. 11. FESEM image of Cr_2O_3-NiO.

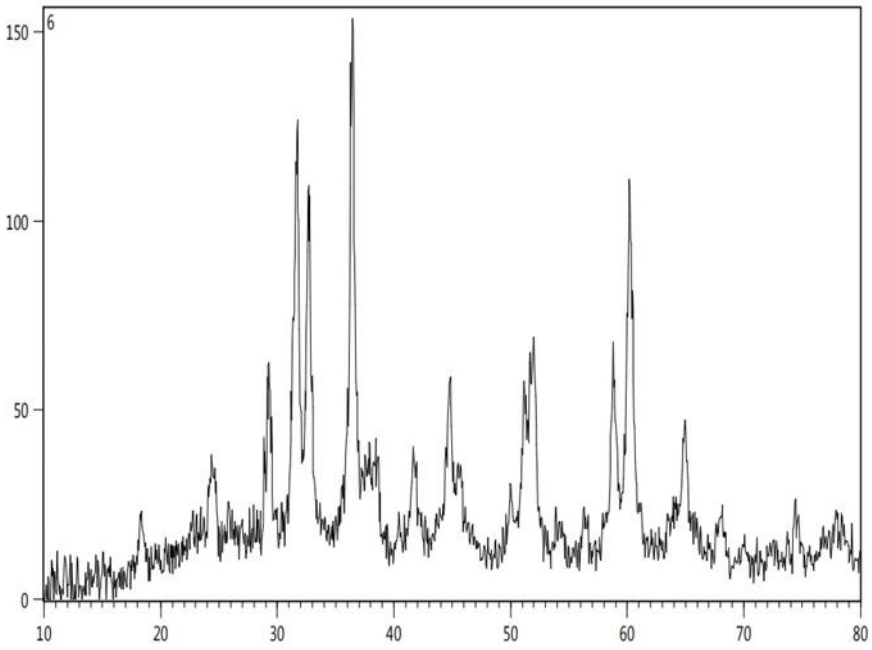

Fig. 12. XRD pattern of rGO.

Spherical shaped formations were aggregated in the form of clusters.

SEM investigation of PANI in Fig. 9 identified plate-like structures in the composition. The generated material displayed a porous structure [25].

According to the Fig. 10, NiO particles were distributed randomly throughout rGO sheet. On the curled morphology of the reduced graphene oxide, NiO particles are dispersed. SEM image show the NiO particles have nanosheet-based irregular structures.

The FESEM micrograph of Cr_2O_3-NiO nanocomposites is shown in Fig. 11. FESEM analysis provides the information about the shape and size. The results of FESEM showed that the average diameter 30-50nm. It can also be seen that the shape of synthesized Cr_2O_3 nanoparticals were homogenous and spherical.

XRD analysis

XRD analysis of rGO is depicted in Fig. 12. The distance between the interlayers was determined to be relatively small compared to graphene oxide, which can be attributed to the removal of a majority of the functional oxygen groups through the process of reduction [26].

Fig. 13 illustrates XRD pattern of synthesized Cr_2O_3 nanoparticles. The diffraction peaks obtained at 2θ =24.5, 33.6, 36.2, 39.7, 41.5, 44.2, 50.2, 54.8, 58.3, 63.4, 65, 72.9, 76.7, and 79.1 degrees, can be related to the Cr_2O_3 standard JCPDS card No. 201103. The standard JCPDS card shows that the alignment of the diffraction peaks perfectly matches the rhombohedral structure of Cr_2O_3 nanoparticles. The results showed that the

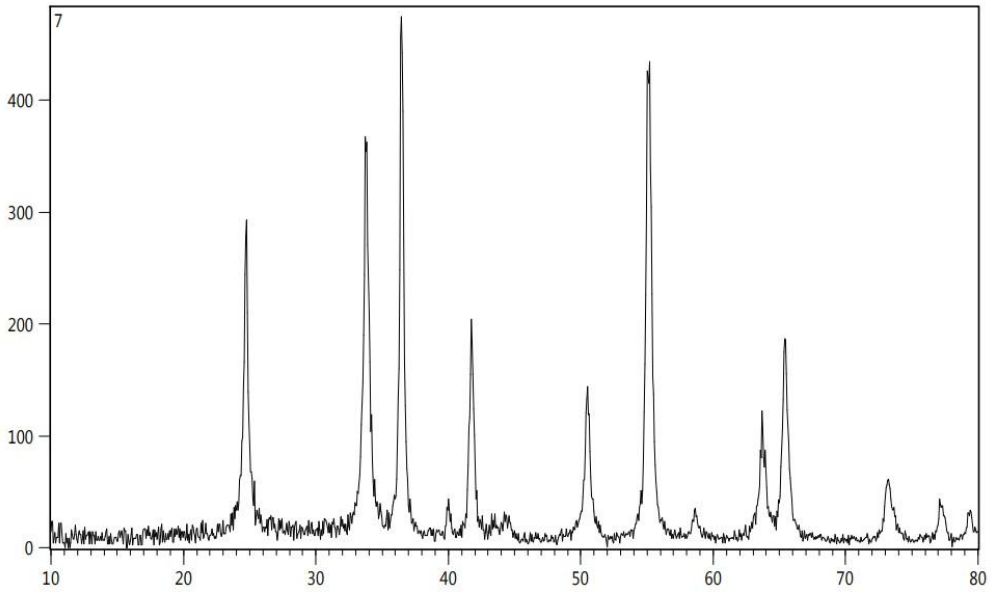

Fig. 13. XRD pattern of Cr_2O_3.

Table 1. The value of ε′ for the synthetized films.

Dielectric Constant (ε′)				
Frequency (MHz)	PVA	PANI/NiO-Cr_2O_3	PANI/rGO-NiO	PANI/rGO-Cr_2O_3
1	3.58787	3.13797	1.69776	1.98913
2	3.52516	2.22089	1.41772	1.72400
3	3.44068	1.84363	1.39226	1.67368
4	3.43068	1.48140	1.35799	1.42774
5	3.4032	1.31134	1.01784	1.26222

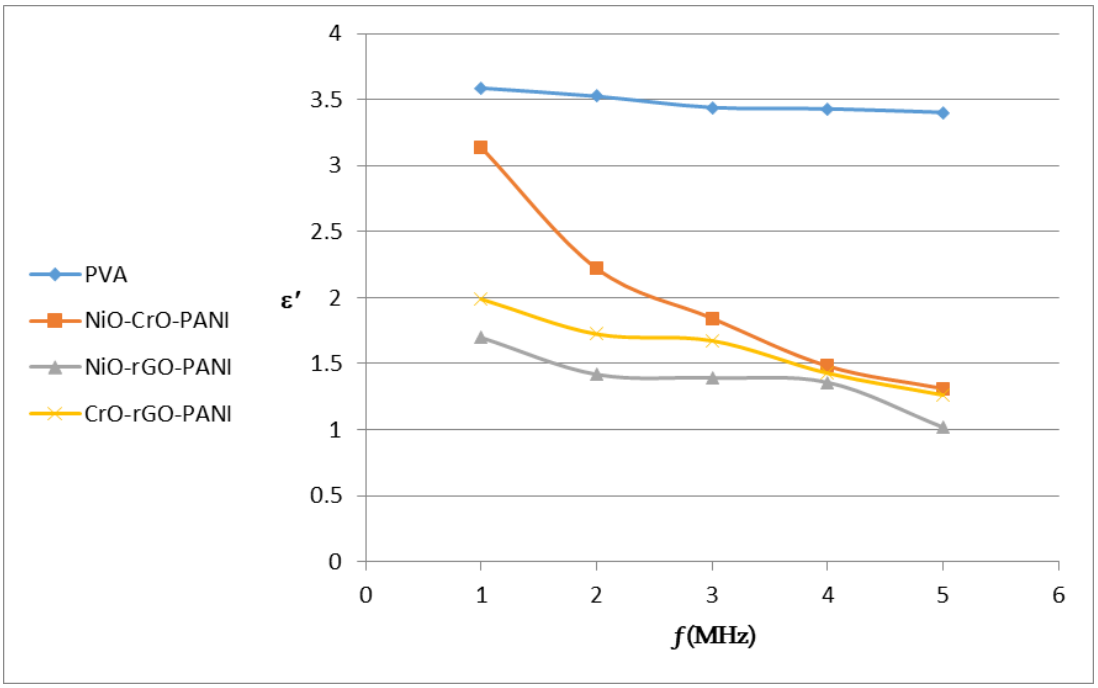

Fig. 14. Real (ε′) dielectric constant of the synthesized hybrid films.

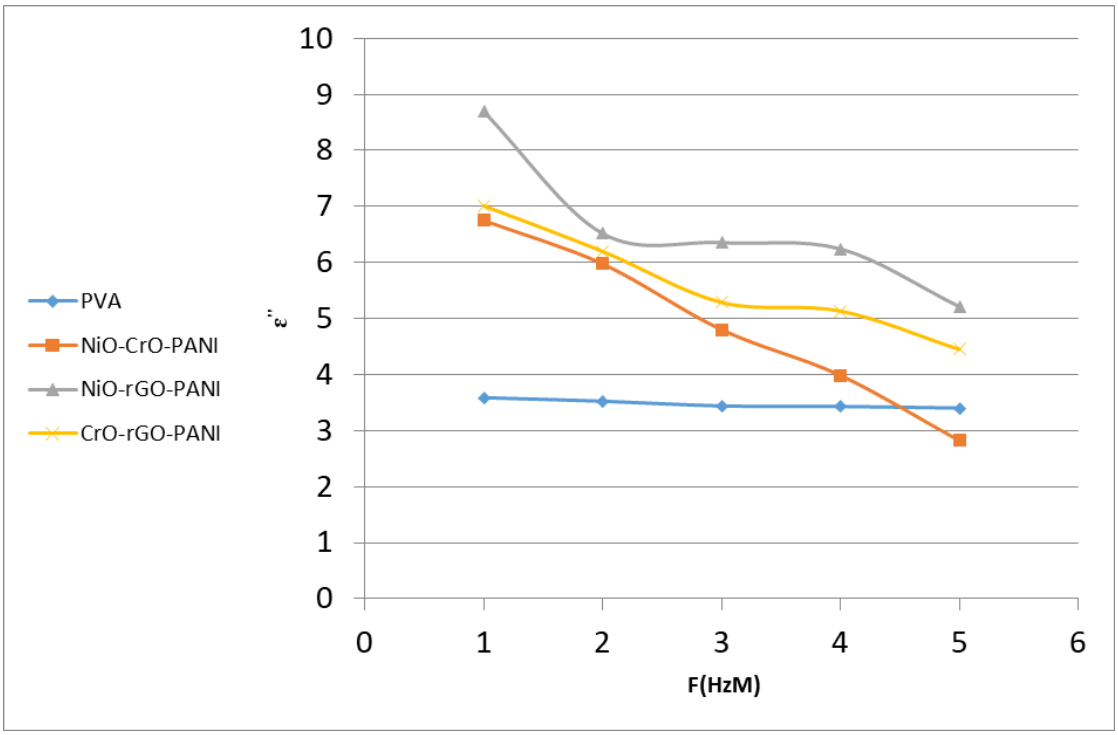

Fig. 15. ε" dielectric constant of the synthesized hybrid films.

synthesized material is completely crystalline [27, 28]. The crystallite size of the Cr_2O_3 was calculated from the Debye-Scherrer formula, and the value is 28 nm.

Dielectric properties

The dielectric properties of the pure PVA polymer film and its hybrid nanocomposite films were determined at room temperature. The results in Figs. 14-16 illustrates that the real permittivity (ε′), imaginary permittivity (ε′′), and loss factor (tanδ=ε′′/ε′) are used as the amount of energy lost or dissipated for any dielectric material and alternating conductivity ($\sigma_{a.c}$). From Table 1, it can be notice both ε′ and ε′′ for all synthesized films were gradually decreased as the frequency increases [29]. Electronic polarization exhibits a brief duration, yet it surpasses ionic polarization in terms of length. On the other hand, dipolar polarization necessitates a comparatively longer time when compared to the other forms of polarization. Thus, the dielectric constant of

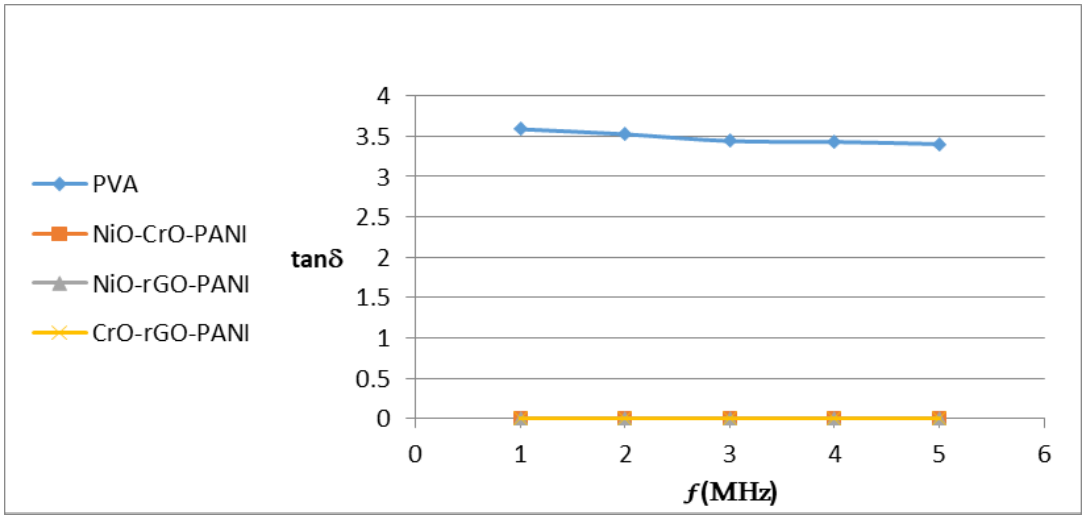

Fig. 16. Dielectric loss factor for the synthesized hybrid films.

Table 2. The value of ε" for the synthetized films.

Frequency (MHz)	PVA	PANI/NiO-Cr_2O_3	PANI/rGO-NiO	PANI/rGO-Cr_2O_3
1	3.58787	6.74882	8.69488	7.01145
2	3.52516	5.97407	6.51698	6.19860
3	3.44068	4.80031	6.35474	5.28774
4	3.43068	3.98488	6.24242	5.1334
5	3.4032	2.82029	5.21275	4.44913

nonpolar polymers remains rather stable at high frequencies. Consequently, the values of ε′ exhibit a substantial and rapid decline as the frequency increases in the low-frequency areas [30]. While frequency ratio of PVA (1MHz) was found to be the dielectric constant's greatest value, while PANI/rGO-NiO was low (5MHz). All of these dielectric constant values exceed the ε′ value for pure PVA. Typically, the rise in the dielectric constant is ascribed to the augmentation in polarity and the growth in charge carriers. Fig. 14 demonstrates a clear inverse relationship between the dielectric loss factor (ε′′) and frequency for all samples. Additionally, we see that the dielectric loss is elevated at lower frequencies and then diminishes as the applied frequency increases, owing to the reduction in space charge polarization. Fig. 15 illustrates that the dielectric loss factor diminishes as frequency increases for synthesized hybrid compounds. This drop is commonly attributed to increasing the concentration of conductive fillers (nanoparticles) which leads to the development of more conductive routes and hence leads to increased current leakage and loss of electrical insulation [21]. Calculations were made to determine the AC electrical conductivity of the pure PVA polymer sheet and all generated hybrid composites. We can see from Fig. 16

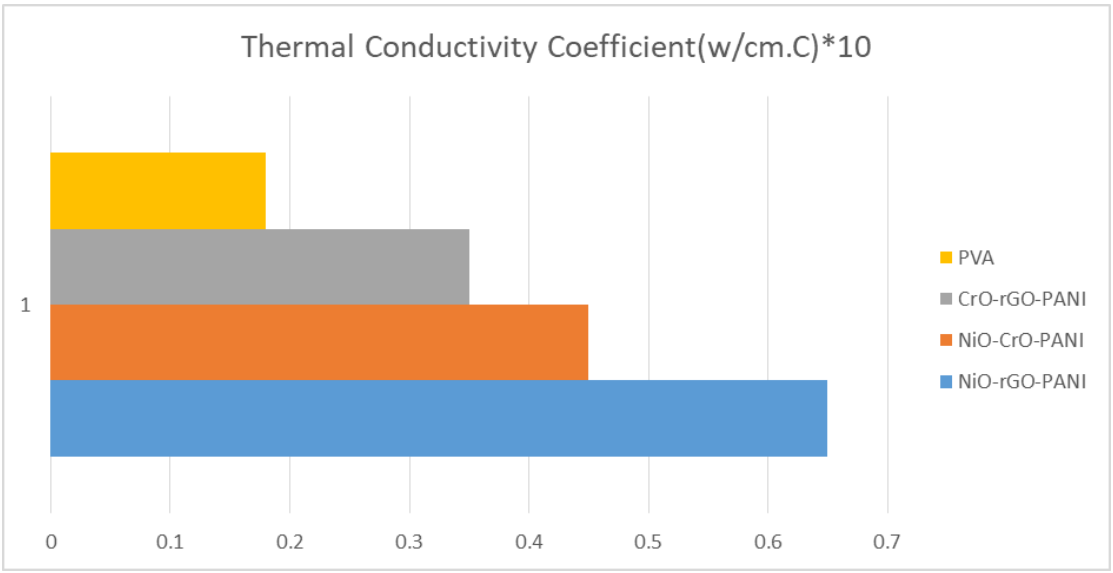

Fig. 17. Thermal conductivity coefficient K for the synthetized films.

Table 3. The value of tanδ for the synthetized films.

f(MHz)	PVA	PANI/NiO-Cr_2O_3	PANI/rGO-NiO	PANI/rGO-Cr_2O_3
1	3.5879	6.7488	8.6949	7.0115
2	3.5252	5.9741	6.517	6.1986
3	3.4407	4.8003	6.3547	5.2877
4	3.4307	3.9849	6.2424	5.1334
5	3.4032	2.8203	5.2128	4.4491

Table 4. The thermal conductivity coefficient K for the synthetized films.

Sample	K(w/cm.c)*10^{-3}	e(w/m^2.k)*10^{-3}
PANI/rGO-NiO	0.65	1.36014
PANI/NiO-Cr_2O_3	0.47	0.28670
PANI/rGO-Cr_2O_3	0.36	0.25441
PVA	0.18	0.02015

that all prepared hybrid composites have an enhancement in isotropic electrical conductivity when nanoparticle is added. This show that the structure contains various conduction mechanisms, which is the (π-π*) interaction between the nanoparticle surface and the quinoid ring of the polymer chain (PANI). This interaction involves electrons passing through the (SP^2-bond), which leads to coupling and electrical conduction. Tables 1-3 lists the values of the real (ε'), imaginary (ε'') dielectric constant, and loss factor (tanδ) for the nano hybrid composite.

Thermal conductivity coefficient

Fig. 17 displays the heat conductivity coefficient of the pure PVA polymer membrane and the nano hybrid composite membranes. By employing nano metal oxides, the thermal conductivity coefficient (k) increases as the reinforcement ratio increases (Table 4). The heat absorption affect the material's ability to conduct heat, thereby increasing its thermal conductivity over time. The elevated temperature of these granules induces their vibration as the temperature increases. The vibration facilitates heat flow across the composite material, enhancing its thermal conductivity. As the proportions of metal oxide, GO, and rGO in the composite material increase, their thermal absorption also escalates, thereby enhancing conductivity. The incorporation of nano oxides may enhance the polymer's crystallization rate, leading to a superior thermal conductivity coefficient compared to a pure PVA polymer film [31].

CONCLUSION

In this work, a ternary polymeric nanocomposite consisting of PANI/rGO-Cr_2O_3, PANI/rGO-NiO, and PANI/NiO-Cr_2O_3 were prepared. The products were characterized using techniques such as FTIR, XRD, FESEM. Finally, the electrical characteristics and thermal conductivity of these materials were examined.

CONFLICT OF INTEREST

The authors declare that there is no conflict of interests regarding the publication of this manuscript.

REFERENCES

1. Darwish A, Ghoniem A, Hassaan MY, El-Said Shehata O, Turky G. Synthesis and Characterization of Polyaniline/Mn_3O_4/ Reduced Graphene Oxide Nanocomposite. Egyptian Journal of Chemistry. 2019;0(0):0-0.
2. Mensing JP, Lomas T, Tuantranont A. Ammonia strengthened graphene/CNT-wrapped polyaniline-nanofiber composites loaded with palladium nanoparticles for coin cell supercapacitors. Electrochimica Acta. 2018;263:17-25.
3. Palsaniya S, Nemade HB, Dasmahapatra AK. Hierarchical Nylon-6/reduced graphene oxide/polyaniline nanocomposites with enhanced dielectric properties for energy storage applications. Journal of Energy Storage. 2020;32:101821.
4. Elahi A, Irfan M, Shakoor A, Niaz NA, Mahmood K, Qasim M. Effect of loading titanium dioxide on structural, electrical and mechanical properties of polyaniline nanocomposites. J Alloys Compd. 2015;651:328-332.
5. Vidya J, Balamurugan P. Synthesis, Structural, Morphological and Optical Characterization of Polyaniline hydrochloride/ Cerium Oxide Nanocomposite. Materials Today: Proceedings. 2019;8:223-230.
6. Izwan Misnon I, Jose R. Charge storage in the PANI–α-MnO_2 polymer–nanocomposite system. Materials Today: Proceedings. 2021;41:513-519.
7. Maruthi N, Faisal M, Raghavendra N, Prasanna BP, Manohara SR, Revanasiddappa M. Anticorrosive polyaniline-coated copper oxide (PANI/CuO) nanocomposites with tunable electrical properties for broadband electromagnetic interference shielding. Colloids Surf Physicochem Eng Aspects. 2021;621:126611.
8. Palsaniya S, Nemade HB, Dasmahapatra AK. Hierarchical PANI-RGO-ZnO ternary nanocomposites for symmetric tandem supercapacitor. Journal of Physics and Chemistry of Solids. 2021;154:110081.
9. Mohammed LA, Majeed AH, Hammoodi OG, Prakash C, Alheety MA, Buddhi D, et al. Design and characterization of

novel ternary nanocomposite (rGO-MnO_2-PoPDA) product and screening its dielectric properties. International Journal on Interactive Design and Manufacturing (IJIDeM). 2022;17(5):2387-2401.
10. Javaherdashti R, Sarjahani R. An Overview of the Effect of Graphene as a Metal Protector Against Microbiologically Influenced Corrosion (MIC). Corrosion Protection of Metals and Alloys Using Graphene and Biopolymer Based Nanocomposites: CRC Press; 2021. p. 149-168.
11. Saif S, Tahir A, Asim T, Chen Y. Plant Mediated Green Synthesis of CuO Nanoparticles: Comparison of Toxicity of Engineered and Plant Mediated CuO Nanoparticles towards Daphnia magna. Nanomaterials. 2016;6(11):205.
12. Alheety NF, Majeed AH, Alheety MA. Silver Nanoparticles Anchored 5-methoxy benzimidazol thiomethanol (MBITM): Modulate, Characterization and Comparative Studies on MBITM and Ag-MBITM Antibacterial Activities. Journal of Physics: Conference Series. 2019;1294(5):052026.
13. Abd AN, Al-Agha AH, Alheety MA. Addition of Some Primary and Secondary Amines to Graphene Oxide, and Studying Their Effect on Increasing its Electrical Properties. Baghdad Science Journal. 2016;13(1):0097.
14. Hummers WS, Offeman RE. Preparation of Graphitic Oxide. Journal of the American Chemical Society. 1958;80(6):1339-1339.
15. Majeed AH, Hussain DH, Al-Tikrity ETB, Alheety MA. Poly (o-Phenylenediamine-GO-TiO_2) nanocomposite: Modulation, characterization and thermodynamic calculations on its H_2 storage capacity. Chemical Data Collections. 2020;28:100450.
16. Synthesis and Characterization of (Go-Mgo-Popda- Pva) Quaternary Nanocomposite Film with Thermal Conductivity Performance. Academic Science Journal. 2024;2(2):172-181.
17. Torrisi L, Silipigni L, Cutroneo M. Radiation effects of IR laser on graphene oxide irradiated in vacuum and in air. Vacuum. 2018;153:122-131.
18. Kadhim K, Agool I, Hashim A. Effect of Zirconium Oxide Nanoparticles on Dielectric Properties of (PVA-PEG-PVP) Blend for Medical Application. Journal of Advanced Physics. 2017;6(2):187-190.
19. Majeed AH, Al-Tikrity ETB, Hussain DH. Dielectric properties of synthesized ternary hybrid nanocomposite embedded in poly (vinyl alcohol) matrix films. Polym Polym Compos. 2020;29(7):1089-1100.
20. Alam SN, Sharma N, Kumar L. Synthesis of Graphene Oxide (GO) by Modified Hummers Method and Its Thermal Reduction to Obtain Reduced Graphene Oxide (rGO)*. Graphene. 2017;06(01):1-18.
21. Aromolaran O. Antimicrobial and synergistic effect of green synthesized silver nanoparticles against multi-drug resistant bacteria. Morressier; 2020.
22. Jayakumar G, Albert Irudayaraj A, Dhayal Raj A. Photocatalytic Degradation of Methylene Blue by Nickel Oxide Nanoparticles. Materials Today: Proceedings. 2017;4(11):11690-11695.
23. Wongsaprom K, Maensiri S. Synthesis and structural characterization of nickel oxide nanoparticles synthesized by Polymerized complexed (PC) method. 2010 3rd International Nanoelectronics Conference (INEC); 2010/01: IEEE; 2010. p. 1044-1045.
24. Bhuiyan MRA, Rahman MK. Synthesis and Characterization of Ni Doped ZnO Nanoparticles. International Journal of Engineering and Manufacturing. 2014;4(1):10-17.
25. Das AK, Sahoo S, Arunachalam P, Zhang S, Shim J-J. Facile synthesis of Fe_3O_4 nanorod decorated reduced graphene oxide (RGO) for supercapacitor application. RSC Advances. 2016;6(108):107057-107064.
26. Latif I, B. Alwan T, H. Al-Dujaili A. Low Frequency Dielectric Study of PAPA-PVA-GR Nanocomposites. Nanoscience and Nanotechnology. 2013;2(6):190-200.
27. Makhlouf SA, Bakr ZH, Al-Attar H, Moustafa MS. Structural, morphological and electrical properties of Cr_2O_3 nanoparticles. Materials Science and Engineering: B. 2013;178(6):337-343.
28. Gibot P, Vidal L. Original synthesis of chromium (III) oxide nanoparticles. J Eur Ceram Soc. 2010;30(4):911-915.
29. Jeevananda T, Siddaramaiah, Kim NH, Heo SB, Lee JH. Synthesis and characterization of polyaniline-multiwalled carbon nanotube nanocomposites in the presence of sodium dodecyl sulfate. Polym Adv Technol. 2008;19(12):1754-1762.
30. Riande E, Diaz-Calleja R. Electrical Properties of Polymers: CRC Press; 2004 2004/05/21.
31. Sharma BK, Khare N, Dhawan SK, Gupta HC. Dielectric properties of nano ZnO-polyaniline composite in the microwave frequency range. J Alloys Compd. 2009;477(1-2):370-373.